

# The Effect of Temperature, Cations, and Number of Acyl Chains on the Lamellar to Non-Lamellar Transition in Lipid-A Membranes: A Microscopic View

Frederico J. S. Pontes, Victor H. Rusu, Thereza A. Soares,\* and Roberto D. Lins\*

Department of Fundamental Chemistry, Federal University of Pernambuco, Cidade Universitária, Recife, PE 50740-560 Brazil

**ABSTRACT:** Lipopolysaccharides (LPS) are the main constituent of the outer bacterial membrane of Gram-negative bacteria. Lipid-A is the structural region of LPS that interacts with the innate immune system and induces inflammatory responses. It is formed by a phosphorylated  $\beta$ -D-glucosaminyl-(1 $\rightarrow$ 6)- $\alpha$ -N-glucosamine disaccharide backbone containing ester-linked and amide-linked long-chain fatty acids, which may vary in length and number depending on the bacterial strains and the environment. Phenotypical variation (i.e., number of acyl chains), cation type, and temperature influence the phase transition, aggregate structure, and endotoxic activity of Lipid-A. We have applied an extension of the GROMOS force field 45a4 carbohydrate parameter set to investigate the behavior of hexa- and pentaacylated Lipid-A of *Pseudomonas aeruginosa* at two temperatures (300 and 328 K) and in the presence of mono- and divalent cations (represented by  $\text{Ca}^{2+}$  and  $\text{Na}^+$ , respectively) through molecular dynamics simulations. The distinct phase of Lipid-A aggregates was characterized by structural properties, deuterium order parameters, the molecular shape of the lipid units (conical versus cylindrical), and molecular packing. Our results show that  $\text{Na}^+$  ions induce a transition from the lamellar to nonlamellar phase. In contrast, the bilayer integrity is maintained in the presence of  $\text{Ca}^{2+}$  ions. Through these findings, we present microscopic insights on the influence of different cations on the molecular behavior of Lipid-A associated with the lamellar to nonlamellar transition.

## 1. INTRODUCTION

The outer membrane of Gram-negative bacteria is composed of an inner leaflet of mainly phosphatidylethanolamine and an outer leaflet of lipopolysaccharide (LPS), which acts as a protective barrier against xenobiotic agents, hydrophobic antibiotics, and the host cells defense system. Besides the functional role as constituents of the outer membrane, LPS is one of the most potent activators of the immune system in mammals, where it stimulates host responses to as few as 100 invading Gram-negative bacteria, the equivalent to femtomolar amounts of endotoxin.<sup>1</sup> Recognition of bacterial virulence factors is the first step for the initiation of an inflammatory and antibacterial immune response. LPS is recognized by a class of transmembrane proteins, the Toll-like receptor family, which has been found to participate in the recognition of bacterial infections.<sup>2</sup> Variations in the LPS structure contribute to bacterial virulence either by dampening early innate immune defense responses to infection<sup>3</sup> or by exacerbating systemic inflammatory responses that ensue when local infection is not contained as in Gram-negative sepsis.<sup>4,5</sup>

The structural region of LPS that interacts with the innate immune system and induces inflammatory responses is known as Lipid-A (Figure 1). In contrast to the role of varying sugar content, alterations of the Lipid-A moiety influence the bioactivity, suggesting that the polysaccharide portion of LPS acts mostly as a solubilizing carrier for the biologically active part.<sup>6,7</sup> Lipid-A anchors the LPS molecule in the membrane and forms a bilayer with the phospholipid inner leaflet of the outer membrane. It is composed of a phosphorylated  $\beta$ -D-glucosaminyl-(1 $\rightarrow$ 6)- $\alpha$ -N-glucosamine disaccharide backbone containing ester-linked and amide-linked long-chain fatty acids that can vary in length and number depending on the bacterial

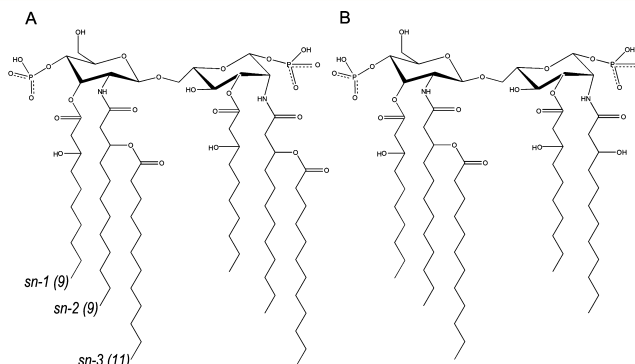


**Figure 1.** Chemical structures of hexa- (A) and pentaacylated (B) forms of Lipid-A. The label in each acyl chain used for the order parameters calculations is indicated in the structure A. The corresponding chain length is shown between parentheses.

strain.<sup>8,9</sup> Lipid-A is the least structurally variable part (chemotype) within the LPS molecule among different species. The most biologically potent Lipid-A is the hexaacylated bisphosphoryl Lipid-A from *Escherichia coli* with a bisphosphorylated diglucosamine backbone (Figure 1).<sup>10</sup>

The biological activity of Lipid-A is critically dependent on specific structural features such as the number of charges, the number and distribution of acyl chains, as well as the supramolecular aggregate structure.<sup>3,11,12</sup> Lipid-A aggregates assume various three-dimensional supramolecular structures as

**Special Issue:** Wilfred F. van Gunsteren Festschrift

**Received:** February 1, 2012

**Published:** May 24, 2012



well as phase states depending on Lipid-A molecular structure (molecular conformation and chemical composition) and ambient conditions (hydration, temperature, type and concentration of cations).<sup>7</sup> Above the critical micellar concentration, Lipid-A may adopt different aggregate structures: lamellar (L), hexagonal ( $H_I$  and  $H_{II}$ ), and cubic (Q). Transitions between these structures can be triggered by changes in the balance between relative attractive and repulsive forces in the headgroup region and in the lipid tails. Overall, the lamellar phase of phospholipids is predominant in functional biological membranes, and although nonlamellar phases are not commonly present *in vivo*, they play a key role as morphological elements required to support the dynamic organization of cellular membrane systems.<sup>13,14</sup> The commonly observed states of the lamellar phase are the lamellar gel phase ( $L\beta$ ), an ordered phase where the acyl chains are in the all-trans conformation, and the lamellar liquid crystalline phase ( $L\alpha$ ), where the conformation and orientation of acyl chains are disordered due to the introduction of *gauche* conformers and undergo fast transitional and rotational diffusion within the plane of the bilayer. Reversible first order  $L\beta \leftrightarrow L\alpha$  transitions occur at a lipid-specific transition temperature ( $T_c$ ), which for Lipid-A exhibits a linear dependency with the number of acyl chains for bisphosphoryl compounds and is also dependent on the nature of mono- and divalent cations.<sup>7,15,16</sup> Furthermore, these phase transitions have been associated with variations in the cross-sectional area of Lipid-A molecules, i.e., in their molecular shape.<sup>6</sup> Since the molecular shape of a given Lipid-A molecule within a supramolecular aggregate is not a constant but depends, at least in part, on the fluidity (inversely correlated to the state of order) of its acyl chains, it is possible to couple molecular conformation (microscopic) with supramolecular structure of the aggregates (macroscopic). Indeed, it is known that the Lipid-A aggregation structure is essential for the expression of endotoxic bioactivity, whereas the state of order of the acyl chains appears to be a modulator of bioactivity.<sup>7,15–18</sup>

We have previously developed an atomistic model<sup>19</sup> for the rough, penta-acylated LPS membrane of *P. aeruginosa*, which has been used to study the structural dynamics of LPS membranes and outer membrane proteins embedded in LPS membranes.<sup>20–24</sup> In this paper, we have used an extension of the GROMOS force field 45a4 carbohydrate parameter set<sup>25</sup> to simulated Lipid-A aggregates with atomistic detail of the structure and interactions. The effect of temperature, nature of cations (mono- versus divalent), and number of acyl chains on the supramolecular structure and phase states of Lipid-A aggregates has been investigated. Our results offer microscopic insight into the molecular behavior of Lipid-A associated with the lamellar → nonlamellar transition.

## 2. METHODOLOGY

**2.1. Simulations Setup.** Initial simulation boxes were comprised of a bilayer structure, where 128 lipids were equally distributed in an  $8 \times 8$  arrangement per layer. In order to neutralize the system, cations were placed in the vicinity of the phosphate groups of Lipid-A molecules. The membranes were then solvated, and water molecules that were eventually placed in the acyl chain regions were physically removed. Boxes of hexaacyl and pentaacyl Lipid-A membrane bilayers were built containing either 128  $\text{Ca}^{2+}$  or 256  $\text{Na}^+$  ions. The systems were geometry optimized using the steepest descent algorithm without constraints for 10 000 steps. The box containing the

hexaacyl Lipid-A bilayer at 300 K was built first, and after reaching equilibration of its potential energy and area per headgroup, one frame was extracted from the trajectory and used as the starting point for all simulations. The system was desolvated, and the number of acyl chains and/or type of counterions was modified accordingly. Each system was then resolvated and equilibration performed. Final simulation box sizes were ca.  $10 \times 10 \times 13$  nm. Simulation lengths were variable due to different equilibration times for each system. A minimum of 50 ns was required to achieve both potential energy and area per headgroup equilibrium.

The simulations were carried out in the isothermal–isobaric ensemble using Berendsen's barostat.<sup>26</sup> A semi-isotropic pressure coupling scheme with a value of 1 bar was controlled by the Berendsen algorithm<sup>26</sup> with a coupling time of 1 ps and compressibility of  $4.5 \times 10^{-10} \text{ m}^2 \text{ N}^{-1}$ . Integration was performed with the leapfrog algorithm<sup>27</sup> with a time step of 1 fs. The temperature was maintained constant by weak coupling to separate heat baths with a relaxation time for the solvent and solute of 0.4 ps using the velocity rescale algorithm.<sup>28</sup> A cutoff of 1.4 nm was used for both short-range electrostatics and van der Waals interactions. Long-range electrostatics was treated via the reaction field method using a permittivity dielectric constant of 66. Periodic boundary conditions were adopted through the simulation, and no constraints were used during the simulations. All simulations were performed using the GROMACS v.4.5.3 simulation package.<sup>29</sup> An extension of the GROMOS force field was used on the basis of the 45a4 carbohydrate parameter set.<sup>25</sup> This extension capitalizes on previously built and validated glucosamine residues<sup>30,31</sup> and encompasses standard bonded parameters between the sugar moiety and the acyl chains as available in the GROMOS 53A6 lipid parameter set.<sup>32,33</sup> The SPC/E<sup>34</sup> water model was used as an explicit solvent. A total of 31 906 molecules were initially placed in each system. Either 128 or 256 water molecules have been replaced by  $\text{Ca}^{2+}$  or  $\text{Na}^+$  ions for the systems containing calcium or sodium as counterions, respectively. A summary of the simulated systems and their temperatures is described in Table 1.

Table 1. Simulated Systems<sup>a</sup>

system	phenotype	counterion	temperature [K]	simulation length [ns] set I/set II <sup>b</sup>
Hexa_Ca_300	hexaacyl	$\text{Ca}^{2+}$	300	250/125
Hexa_Na_300	hexaacyl	$\text{Na}^+$	300	137/125
Hexa_Ca_328	hexaacyl	$\text{Ca}^{2+}$	328	180/125
Penta_Ca_300	pentaacyl	$\text{Ca}^{2+}$	300	118/125
Penta_Na_300	pentaacyl	$\text{Na}^+$	300	108/125

<sup>a</sup>Lipid-A bilayers differ in number of acyl chains, type of cations, and temperature. <sup>b</sup>For details, see section 3.7.

**2.2. Data Analysis.** Despite the different simulation times for each system (over 100 ns for all cases), the MD-derived properties<sup>35,36</sup> were analyzed for the last 50 ns of simulations, and averages were calculated over 128 Lipid-A molecules. The remaining simulations were treated as an equilibration phase, even though convergence of the potential energy and area per headgroup may have occurred much earlier for some cases. The area per headgroup was calculated by dividing the box dimension in the  $x$ - $y$  axis by the total number of Lipid-A molecules in one leaflet of the bilayer. Mass partial densities of

cations, phosphorus atoms, oxygen atoms from water, and acyl chains were calculated along the  $z$  axis of the simulation box, i.e., the normal axis to the bilayer. The glucosamine average tilt angle with respect to the membrane plane was computed as the average complementary angle between the  $z$  axis and the vector that connects the Lipid-A glucosamines for 128 Lipid-A molecules. The Lipid-A angle orientation was calculated as the angle between the  $z$  axis and the vector that connects the center of masses of the acyl chain methylene carbon atoms and the glucosamine ring for each Lipid-A molecule. The ratio between the radius of gyration of the glucosamine residues and the methyl groups was calculated for 128 molecules. Radial distribution functions were calculated between three pairs: (i) phosphorus and water oxygen atoms, (ii) the phosphorus atom and cation, and (iii) the cation and water oxygen atom. Deuterium order parameters  $S_{CD}$  for the acyl chains were calculated from the elements of the order parameter tensor and estimate the average orientation of the hydrophobic chain. The order parameter elements are defined as  $S_{CD} = \langle (3 \cos^2 \theta - 1)/2 \rangle$ .  $\theta$  is the angle between the molecular axis given by two consecutive carbon atoms and the lipid bilayer normal plane. If the lipids chains are perfectly ordered in the membrane, the angle between the C–D bonds in the acyl chain and the bilayer normal will be  $90^\circ$  with  $S_{CD} = -0.5$ . A value of  $S_{CD} = 0$  corresponds to an orientation of the C–D bond that is either permanently at an angle of  $0^\circ$  or random. Because lipid tails in membranes are on average aligned along the bilayer normal, typical  $S_{CD}$  values are between 0 and  $-0.5$ , with  $-0.5$  indicating maximum order.  $S_{CD}$  values are usually reported as  $-S_{CD}$  or  $|S_{CD}|$ . As the GROMOS force field uses a united-atom representation, the positions of the deuterons were constructed on the basis of the positions of the neighboring carbons assuming tetrahedral geometry. Glucosamine and molecular tilt angles were calculated using in-house developed programs (available for download at <http://dqfnet.ufpe.br/biomat>). All of the other analyses as well as simulations were made with the GROMACS v.4.5.3 simulation package.<sup>29</sup>

### 3. RESULTS AND DISCUSSION

The results herein presented aim to establish a relationship between mono- versus divalent cations, temperature, and the number of acyl chains on the structural dynamics of Lipid-A aggregations. Data analyses are presented for the last 50 ns of simulation time for each system, unless otherwise noted.

**3.1. Atom Density Profiles.** Density profiles of selected chemical groups such as acyl chain methylene, cations ( $\text{Ca}^{2+}$  or  $\text{Na}^+$ ), water oxygen, and phosphate phosphorus atoms along the transmembrane axis were calculated for the simulated systems (Figure 2). Such distribution can be compared to neutron and X-ray diffraction measurements in order to infer the influence of the different cations on aggregate structure. The atom density distributions for the systems in the presence of  $\text{Ca}^{2+}$  cations exhibit a symmetrical pattern for all selected chemical groups (Figure 2A, B, and C). This symmetry is characteristic of a lamellar arrangement, indicating that in the presence of  $\text{Ca}^{2+}$  cations both penta- and hexaacyl Lipid-A adopt a bilayer structure. The temperature increase from 300 K to 328 K does not affect significantly the distribution of the chemical groups along the normal membrane axis, except for a slightly smoother distribution (compare Figure 2A and B). Although water molecules are absent of the central trough corresponding to methylene groups in the Lipid-A acyl chains, the bilayer is fairly permeable with water molecules penetrating

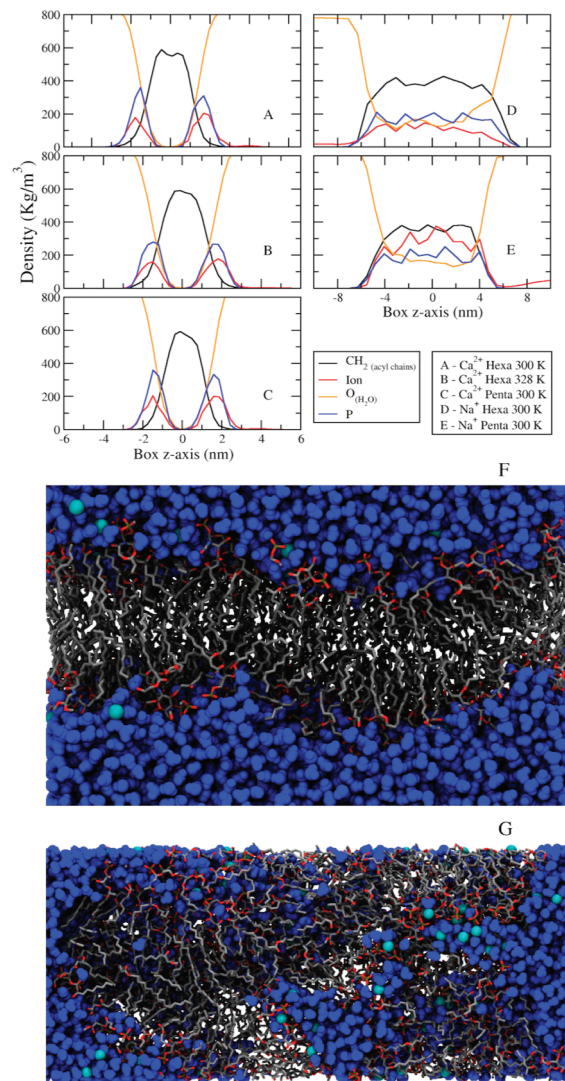


**Figure 2.** (A–E) Partial number density along the membrane normal axis of selected chemical groups in the Lipid-A bilayer. Values are averaged over 128 Lipid-A molecules over the last 50 ns of simulation. (Density values for phosphorus atoms (P) and ions have been increased by 5 fold for clarity). (F and G) Lamellar and nonlamellar phases depicted by molecular representation of the representative structures for systems A and D, respectively. The molecular model for Lipid-A membranes is shown in stick (with atoms color coded as red, oxygen; gray, carbon; blue, nitrogen; orange, phosphate; hydrogens are omitted for clarity) and water molecules and counterions ( $\text{Na}^+$  and  $\text{Ca}^{2+}$ ) in the CPK model colored in blue and cyan, respectively.

the outward region of the hydrophobic core. This is in agreement with neutron diffraction measurements performed for LPS membranes of *Pseudomonas aeruginosa*.<sup>37,38</sup> However, Lipid-A bilayers appear to be even more permeable than LPS bilayers given that water molecules penetrate the former up to 10 Å from its center compared to the estimated distance of 22 Å for the latter.<sup>37,38</sup> The higher permeability of Lipid-A can be ascribed to the lack of the keto-d-octulosonic acid (KDO) group and remaining carbohydrates of the inner core, the outer core, and O-antigen composing the LPS membranes. These missing carbohydrate moieties function as a physical barrier due to the stronger binding of  $\text{Ca}^{2+}$  to the KDO carboxylate groups ( $k_d = 6 \mu\text{M}$ ) compared to  $\text{Ca}^{2+}$  binding to the glucosamine phosphate group ( $S_6-100 \mu\text{M}$ ) in Lipid-A.<sup>39</sup> This difference is

further accentuated by the presence of a higher number of  $\text{Ca}^{2+}$  binding sites represented by the extra charged groups (the carboxylates of the KDO moieties and phosphates attached to the heptose sugars) in the LPS membranes.

A distinct situation is observed for the penta- and hexaacyl Lipid-A in the presence of  $\text{Na}^+$  cations where water molecules, cations, and glucosamine (represented by the position of the phosphorus atoms) are spatially distributed throughout the entire simulation box (Figure 2D and E). In the presence of  $\text{Na}^+$ , both penta- and hexaacyl Lipid-A bilayers transition from a lamellar to a nonlamellar arrangement. Figure 2F and G illustrate the molecular representations of lamellar and nonlamellar phases as obtained in the hexaacyl simulations in the presence of  $\text{Ca}^{2+}$  and  $\text{Na}^+$  ions at 300 K, respectively. It is remarkable that while the Lipid-A bilayer arrangement is disrupted in the  $\text{Na}^+$ -containing simulations at 300 K, the same arrangement is preserved in  $\text{Ca}^{2+}$ -containing systems at 328 K.

**3.2. Area per Lipid  $A_L$ .** The area per lipid was calculated for the lamellar systems, i.e., penta- and hexaacyl Lipid-A in the presence of  $\text{Ca}^{2+}$  at temperatures of 300 K and 328 K (Figure 3). Average values are  $1.54 \text{ nm}^2$  (300 K) and  $1.57 \text{ nm}^2$  (328 K)

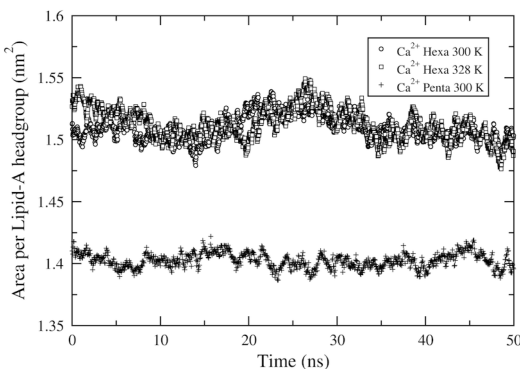


Figure 3. Area per lipid molecule as a function of time for Lipid-A membranes in the lamellar phase as a function of time.

for the hexaacyl Lipid-A and  $1.42 \text{ nm}^2$  (300 K) for the pentacyl Lipid-A. Experimental estimates of the area per lipid for Lipid-A in the gel phase range between  $1.25 \text{ nm}^2$  (293.15 K) and  $1.30 \text{ nm}^2$  (313.15 K).<sup>40</sup> Values for Lipid-A in the liquid crystalline phase are not available. For comparison purposes, experimental values for LPS in the liquid-crystalline phase are taken as a reference.<sup>40,41</sup> Brandenburg et al.<sup>40</sup> estimated the area per lipid for several LPS chemotypes from *Salmonella minnesota* as varying between  $1.29 \text{ nm}^2$  and  $1.42 \text{ nm}^2$  depending on the completeness of the sugar moieties, e.g., from the shortest rough LPS up to the smooth LPS chemotypes. Snyder et al.<sup>41</sup> estimated the area per acyl chain in the liquid crystalline phase for LPS membranes of two *Salmonella* strains (*minnesota* R7 and *typhimurium* SL848) containing both rough and smooth LPS chemotypes as  $0.26 \text{ nm}^2$ , which can be converted to values of area per lipid of  $1.56 \text{ nm}^2$  and  $1.30 \text{ nm}^2$  for the hexaacyl and pentacyl forms, respectively. It is worth noting that the larger transmembrane section area of the LPS is by far due to the Lipid-A part, so its area may fair well relative to its rough chemotype counterpart. On the other hand, the presence of the O-antigen chain (smooth chemotype) may affect the overall fluidity, dynamics, and lateral diffusion, therefore increasing the area per lipid.<sup>21</sup>

Comparison between calculated and experimental values of the area per lipid indicates that all  $\text{Ca}^{2+}$ -containing systems

simulated are in the liquid-crystalline phase. Calculated values are closer to the area per lipid measured from LPS membranes of *P. aeruginosa* than from those of *S. minnesota*. This is expected because the acyl chain of the simulated Lipid-A has the same length as those of *P. aeruginosa* (10–12 carbon atoms) whereas *S. minnesota* has longer acyl chains (14–16 carbon atoms).<sup>40,42</sup> Lipid-A with short acyl chains exhibits lower phase transition temperatures, e.g.,  $T_c < 293.15 \text{ K}$  for 10–12 carbon atoms and  $T_c > 315.15 \text{ K}$  for 14–16 carbon atoms.<sup>43</sup> Furthermore, the area per lipid is nearly identical for the hexaacyl Lipid-A at 300 K and 328 K, suggesting that the gel  $\leftrightarrow$  liquid-crystalline transition should take place at lower temperature values for these Lipid-A membranes.

### 3.3. Diglucosamine Tilt Angle and Gyration Radius Ratio

**Ratio.** The molecular conformation and supramolecular structure of Lipid-A aggregates are a prerequisite for the expression of endotoxicity.<sup>10,17,44,45</sup> FTIR spectroscopy measurements were previously used to estimate the orientation of molecular groups within Lipid-A, which has been interpreted in terms of two main conformations with a range of variations in between the two geometries.<sup>45</sup> The conformation of highest endotoxicity is conical-shaped due to the higher cross-section of the hydrophobic moiety with respect to the hydrophilic moiety of the Lipid-A, and the tilt angle between the diglucosamine backbone with respect to the direction of the hydrocarbon chains has large values (ca.  $50^\circ$ ), whereas the endotoxically inactive conformation is cylindrical-shaped with nearly equivalent cross-section values of the hydrophobic and the hydrophilic moieties of the Lipid-A molecule and small tilt angle values (< $25^\circ$ ; see Figure 5 for an illustration of the molecular shapes).<sup>45</sup>

The tilt angle between the vector that connects the center of mass of each diglucosamine and the bilayer surface plane was calculated along the last 50 ns of simulation for the lamellar systems (Figure 4). Analysis of time-dependent and distribution patterns for this property shows that the increase of the temperature from 300 K to 328 K or the decrease of the number of acyl chains (penta versus hexaacyl) leads to a consistent, but small, variation (ca.  $2^\circ$  to  $3^\circ$ ) of the glucosamine tilt angle with respect to the membrane plane. Calculated average values of tilt angles for the lamellar Lipid-A simulations

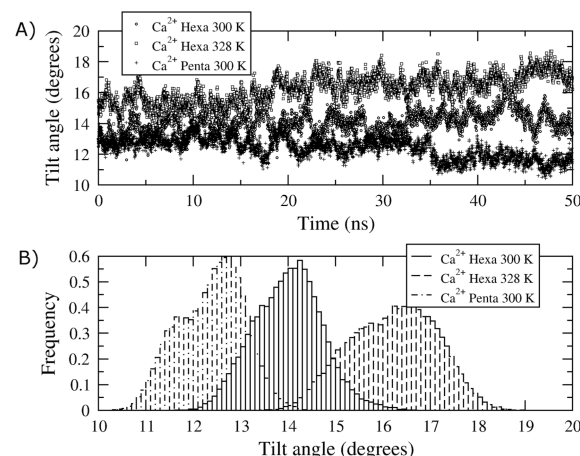
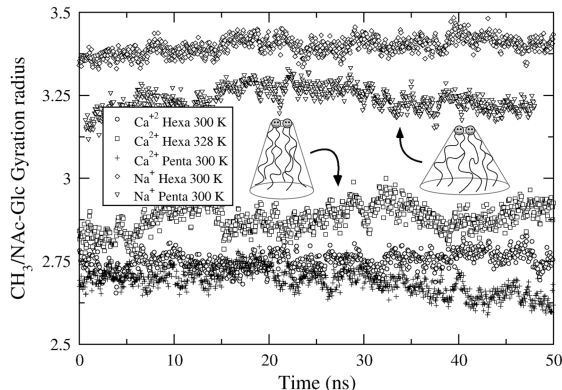


Figure 4. Lipid-A glucosamine tilt with respect to the  $z$  axis for lamellar systems. (A) Average values over 128 lipids are presented as a function of the last 50 ns of simulation time for each system and (B) their distribution binned at each  $0.1^\circ$ .

are ca. 12° to 17° depending on the number of acyl chains and temperature. Experimental estimates of the tilt angle for penta- and hexacyl Lipid-A varies greatly with large errors associated with the measurements (see Table 1 of Seydel et al.<sup>45</sup> Notwithstanding, the calculated values are in excellent agreement with the average experimental values, which are in the range of 10–15° for the pentaacetyl and hexaacyl forms with a symmetrical distribution of acyl chains.<sup>45</sup>

The molecular shape of Lipid-A can also be deduced from its aggregate structure where Lipid-A molecules adopt a cylindrical shape in lamellar arrangements and a conical geometry in nonlamellar arrangements.<sup>7,10,44</sup> Therefore, a direct correlation can be established between the Lipid-A molecular structure and its aggregate supramolecular structure.<sup>10,44,46</sup> In order to determine the molecular shape of the individual Lipid-A molecules in the lamellar and nonlamellar simulated systems, the ratio between the radius of gyration of the glucosamine residues and the methyl groups was calculated for each Lipid-A system as a function of the last 50 ns of simulation (Figure 5).



**Figure 5.** Ratio between the radius of gyration of the acyl chain methyl groups ( $\text{CH}_3$ ) and the glucosamine residues in each Lipid-A molecule. Values are presented as a function of the last 50 ns of simulation time for each system and were averaged over the values for 128 lipids.

The gyration radius ratio of Lipid-A molecules in  $\text{Na}^+$ -containing systems is ca. 20% larger than those calculated for the lamellar systems in the presence of  $\text{Ca}^{2+}$  (Figure 5). This is consistent with the nonlamellar supramolecular structure observed for these simulations and with the fact that monovalent salts of LPS exhibit the strongest endotoxicity.<sup>47</sup> All lamellar systems exhibit similar values for the gyration radius ratio. This property shows a small increase for the hexaacyl Lipid-A upon a temperature increase from 300 K to 328 K and a small decrease for the pentaacyl Lipid-A bilayer compared to the hexaacyl form at 300 K.

A sharp distinction between molecular shapes can be made between  $\text{Na}^+$ - and  $\text{Ca}^{2+}$ -containing Lipid-A (Figure 5). It can be seen that in the presence of  $\text{Ca}^{2+}$ , Lipid-A adopts a more cylindrical molecular shape, favoring lamellar aggregate structures, whereas in the presence of  $\text{Na}^+$ , it favors a more conical molecular shape and nonlamellar aggregate structures. It should be noticed that the experimental characterization of the intrinsic conformation of Lipid-A (molecular shape) and its aggregate structure as a function of the number of acyl chains and temperature have been performed in the presence of  $\text{Mg}^{2+}$  and not  $\text{Ca}^{2+}$  cations.<sup>6,7,10,44–46</sup> However, LPS in the presence of  $\text{Ca}^{2+}$  cations is orders of magnitude less endotoxic than in the presence of  $\text{Mg}^{2+}$  cations and even more than in the

presence of  $\text{Na}^+$ .<sup>38,47</sup> These findings are consistent with our estimates of Lipid-A adopting a cylindrical (endotoxically inactive) or conical (endotoxically active) molecular shape depending on the presence of  $\text{Na}^+$  or  $\text{Ca}^{2+}$  cations, respectively.

**3.4. Radial Distribution Function.** The lamellar to nonlamellar transition upon replacement of  $\text{Ca}^{2+}$  by  $\text{Na}^+$  ions indicates that the event is driven by the interaction of the cations with the Lipid-A headgroups. Radial distribution functions (RDF) of the cations and oxygen atoms with respect to the phosphate groups (represented by the phosphorus atoms) were calculated to characterize the interaction pattern between cations and Lipid-A headgroups (Figure 6). The

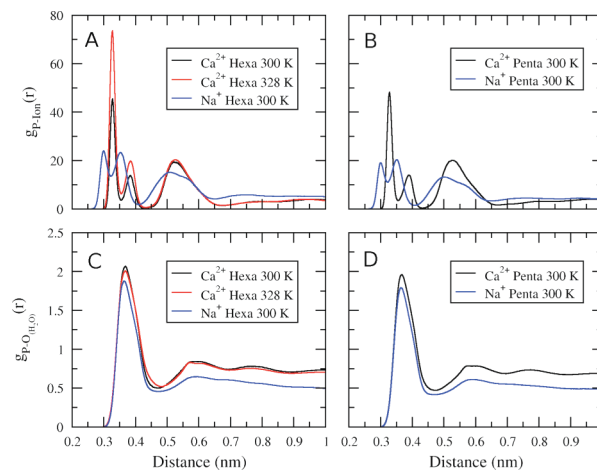


**Figure 6.** Radial distribution function between (A, B) ions and phosphorus atoms and (C, D) phosphorus atoms and water oxygen in the hexaacyl (left) and pentaacyl (right) Lipid-A simulations. Values were averaged over the last 50 ns of simulation time for each system.

phosphorus–cation profiles for the penta- and hexaacyl Lipid-A systems are nearly identical in the presence of  $\text{Ca}^{2+}$  cations and at 300 K (Figure 6A and B). The temperature increase to 328 K for the hexaacyl Lipid-A system in the presence of  $\text{Ca}^{2+}$  ions causes changes solely in the peak intensities, preserving the pattern profile (Figure 6A). For the  $\text{Ca}^{2+}$ -containing system at 300 K, the phosphorus–cation RDF integrals until the first, second, and third peaks are 0.13, 0.22, and 0.98, respectively, and at 328 K, the integrals are 0.22, 0.35, and 1.14, respectively (Figure 6A). The corresponding RDF integrals until the first, second, and third peaks for  $\text{Na}^+$ -containing systems at 300 K are 0.15, 0.52, and 1.14 (Figure 6B). It is worth noting that the first two peaks of the phosphorus–cation profiles for the penta- and hexaacyl Lipid-A (Figure 6A and B) have integrals below one and RDF values above one. It shows phosphorus–cation interactions in lengths below the average value of ca. 0.52 nm (for  $\text{Ca}^{2+}$ -containing systems) and ca. 0.45 nm (for  $\text{Na}^+$ -containing systems). These peaks indicate that cations tend to cluster around Lipid-A phosphate groups in a noncrystalline manner. This behavior has been previously reported in simulations of a lipopolysaccharide membrane of *P. aeruginosa* in the presence of  $\text{Ca}^{2+}$  ions.<sup>19,20,23</sup> The third peak for the  $\text{Ca}^{2+}$ - and  $\text{Na}^+$ -containing systems represents one  $\text{Ca}^{2+}$  bridging two phosphate groups and two  $\text{Na}^+$  bridging two phosphate groups in different Lipid-A molecules. On average, each  $\text{Na}^+$  ion coordinates a sole phosphate group with about two cations in between neighboring Lipid-A molecules. The two closer peaks at ca. 0.29 and 0.36 nm for the  $\text{Na}^+$  cations with respect to the phosphate phosphorus atoms is due to the monovalent charge

and the smaller ionic radius of  $\text{Na}^+$  compared to the two peaks at ca. 0.32 and 0.38 nm of the  $\text{Ca}^{2+}$  cations. The third peak is broader in the  $\text{Na}^+$ -containing systems compared the corresponding one for the systems in the presence of  $\text{Ca}^{2+}$  ions. The radial distribution functions of the phosphorus and water oxygen atoms (Figure 6C and D) exhibit a first peak at ca. 0.36 nm, which differ in their intensities for the  $\text{Ca}^{2+}$ - and  $\text{Na}^+$ -containing systems (Figure 6C and D). A clearly defined second peak is absent in the  $\text{Na}^+$ -containing systems, as expected for a nonlamellar arrangement. The integral of the RDF curves gives an average number of 8 and 7 water molecules per phosphate group (represented by its phosphorus atom) in the presence of  $\text{Ca}^{2+}$  and  $\text{Na}^+$  cations, respectively. These findings suggest that water molecules have been partly displaced during the lamellar to nonlamellar transition. This is in agreement with the fact that each cation replaces one water molecule and that there are two  $\text{Na}^+$  ions nearby a couple of phosphate groups, oppositely to only one  $\text{Ca}^{2+}$  per two phosphates.

**3.5. Deuterium Order Parameter  $S_{CD}$ .** The deuterium order parameters  $S_{CD}$  of the *sn*-1, *sn*-2, and *sn*-3 acyl chains of Lipid-A were calculated for the  $\text{Ca}^{2+}$ - and  $\text{Na}^+$ -containing systems (Figure 7).  $S_{CD}$  measures the relative orientation of the

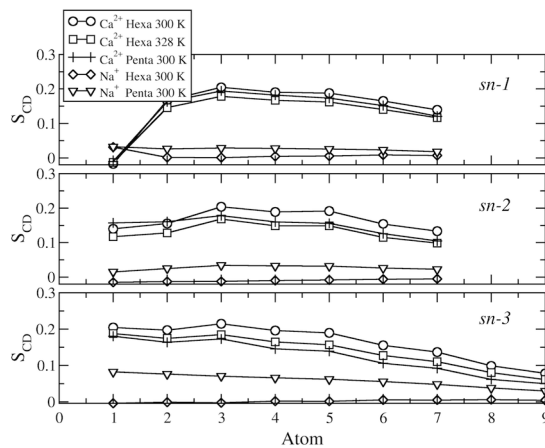


**Figure 7.** Carbon-deuterium order parameter ( $S_{CD}$ ) for carbon atoms in the acyl chains of the Lipid-A membranes (see Figure 1 for acyl chain number assignments). Order parameter values were averaged over 128 LPS molecules over the last 50 ns of simulation time for each system. Values are plotted as a function of the carbon sequence number in acyl chains.

C–D bonds with respect to the bilayer normal. The degree of order-disorder of acyl chains can be associated with their mobility or fluidity (inversely proportional to the state of order). In the  $\text{Ca}^{2+}$ -containing systems, the  $S_{CD}$  values are lower than 0.23 with an increasing disorder along the aliphatic chains toward the methyl groups (Figure 7). This profile is due to the tethering and alignment of the acyl segments near the aqueous interface, with increased disorder in the bilayer center due to the flexibility of the chain termini. In the  $\text{Na}^+$ -containing systems, the  $S_{CD}$  values are near or at 0 with a much flatter profile. This is expected due the disappearance of the lamellar arrangement. Despite the distinct pattern for  $\text{Ca}^{2+}$ - and  $\text{Na}^+$ -containing Lipid-A aggregates, the variation of the temperature and number of acyl chains does not show a significant effect on  $S_{CD}$  values. In any case, the trend in all  $\text{Ca}^{2+}$ -containing simulations is a slightly less ordered hexaacyl Lipid-A

membrane at 328 K and much alike disordered penta- and hexaacyl Lipid-A at 300 K.

$S_{CD}$  values are not available for LPS and Lipid-A membranes. Instead, it is possible to quantify the orientation of molecules from polarized IR spectra of oriented samples from the peak position of the symmetric stretching vibration,  $\nu_s$ , of the methylene groups around  $2850 \text{ cm}^{-1}$ , as determined by attenuated total reflectance measurements coupled to Fourier transform infrared (ATR-FTIR) spectroscopy. To establish an approximation for the order parameter, fluorescence polarization experiments with standard phospholipids like dipalmitoyl-glycerophosphocholine were correlated with corresponding infrared data, allowing the establishment of a correlation between  $\nu_s$  and  $S_{CD}$ . A curve fitting has been proposed on the basis of the following third order polynomial:

$$S = -941.8 + 0.7217\nu_s - 7.823E - 05\nu_s^2 - 2.068E - 08\nu_s^3$$

This estimate named  $S$  assumes values, like for  $S_{CD}$ , between  $S = 1$  for perfectly aligned acyl chains and  $S = 0$  for isotropic systems.  $S$  values for short acyl chains Lipid-A as the simulated systems are on the order of 0.28 (*P. aeruginosa*), 0.27 (*Rhodobacter capsulatus*), and 0.15 (*Rhodococcus gelintinosus*).<sup>43</sup> Therefore, the calculated  $S_{CD}$  values are within the range of experimental  $S$  values. Consistently with the calculated area per lipid, the calculated  $S_{CD}$  values are typical of the  $\text{L}\alpha$  phase (liquid-crystalline). An  $\text{L}\beta \leftrightarrow \text{L}\alpha$  transition was not observed either from penta- to hexaacyl at 300 K or from 300 to 328 K for the hexaacyl Lipid-A (Figure 7). These results suggest that  $\text{L}\beta \leftrightarrow \text{L}\alpha$  phase transition for Lipid-A from *P. aeruginosa* takes place at a lower temperature. Although the experimental values of phase transition temperature could not be found for *P. aeruginosa*, it is supported by fact that a number of Lipid-A membranes from different organisms do have transition temperatures below 20 °C (293.15 K)<sup>43</sup> and the first order linear dependency of  $\text{L}\beta \leftrightarrow \text{L}\alpha$  transitions with the number of acyl chains.<sup>7,15,16</sup> A general behavior dictates that the shorter the length of the acyl chain, the lower is the corresponding phase transition temperature. In addition, the  $\text{L}\beta \leftrightarrow \text{L}\alpha$  phase transition for LPS membranes of *P. aeruginosa* occurs continuously over a range of temperatures, without the typical sharp transition observed for phospholipids and enterobacterial LPS membranes.<sup>37,41,43</sup> Therefore, the most plausible interpretation for that is again that all three systems are in a liquid-crystalline phase. Ongoing efforts will address this issue in the near future.

A significantly higher degree of disorder can be seen from the calculated  $S_{CD}$  values for the  $\text{Na}^+$ -containing systems (Figure 7). Contrasting with the lamellar  $\text{Ca}^{2+}$ -containing systems,  $S_{CD}$  values are lower for hexaacyl than for pentacyl Lipid-A for all (*sn*-1, *sn*-2, and *sn*-3) chains. This is in agreement with the observation that on average hexaacyl Lipid-A favors nonlamellar arrangements, whereas pentacyl Lipid-A favors the formation of lamellae (see Table 2 in Brandenburg et al.<sup>43</sup>). These results evidence a distinct structural dynamical behavior of the acyl chains in lamellar and nonlamellar systems, which should be put into perspective regarding transitions within the same aggregate structure versus transitions from different aggregate structures. Hence, the  $S_{CD}$  values calculated for the  $\text{Ca}^{2+}$ -containing systems present an assessment of  $\beta \rightarrow \alpha$  phase transition (not observed in our simulations), whereas the  $S_{CD}$  values for the  $\text{Na}^+$ -containing systems probe the lamellar →

nonlamellar transition (observed in our simulations). It is known that the  $\beta \leftrightarrow \alpha$  phase transition of acyl chains in Lipid-A aggregates can either take place within the same aggregate arrangement or can be connected with a transition between different aggregate structures.<sup>48</sup>

**3.6. Orientation of Lipid-A Molecules in the Aggregates.** Nonlamellar aggregates of Lipid-A can occur in different forms ( $Q_1 H_1 H_{II}$ ) depending on a variety of factors.<sup>15,48,49</sup> The tilt angle between a vector along the longest axis of each Lipid-A molecule and membrane plane (as defined from the initial configuration of each system) was calculated to structurally characterize the lamellar to nonlamellar transition observed for  $Na^+$ -containing Lipid-A aggregates (Figure 8A). Angle values range from  $0^\circ$  (with molecules parallel to the  $z$  axis) to  $90^\circ$  (with molecules perpendicular to the  $z$  axis). In an ideal crystalline-phase membrane, the average lipid orientation would be at  $0^\circ$ . However, a certain level of tilt would be expected for a real system, especially if in the liquid-crystalline phase. In the case of an ideal micelle, tilt angles would cover values in the

entire range from  $0^\circ$  to  $90^\circ$  with equal frequency. On average, the calculated tilt angle values for Lipid-A in presence of  $Ca^{2+}$  varies between  $15^\circ$  and  $20^\circ$  as expected for a lamellar arrangement (Figure 8A). Nonetheless, there is a fair occurrence of angle values over  $45^\circ$ , which increases when the temperature is raised from 300 K to 328 K. A shift in the average tilt value from ca.  $15^\circ$  to  $20^\circ$  is also observed. Despite a frequency near 20% of molecules tilted into a herein-defined nonlamellar configuration, Lipid-A aggregates behave as typical lamellar bilayers in the presence of  $Ca^{2+}$  cations, as seen from MD snapshots (Figure 8B). The coexistence of diverse molecular orientations within the Lipid-A bilayer offers a microscopic insight into complex structural polymorphism experimentally described for Lipid-A aggregates.<sup>15,48,49</sup>

The presence of  $Na^+$  cations causes a dramatic shift in the Lipid-A tilt angle values for both penta- and hexaacyl forms (Figure 8A). Due to the use of an asymmetric pressure scaling scheme, the size of our simulation box, and possibly simulation time, a perfect single micelle would be hardly observed. However, visual inspection of the MD trajectories reveals a clear transition from lamellar to cubic arrangement in the presence of  $Na^+$  ions. A depiction of such a scheme as well as snapshots from the beginning and the end of the hexaacyl Lipid-A simulation in the presence of  $Na^+$  ions are presented (Figure 8B). The same behavior is observed for the pentaacyl systems (not shown for conciseness).

**3.7. Cation Influence on the Supramolecular Structure of Lipid-A.** Although  $Ca^{2+}$  and  $Na^+$  cations are ubiquitous and abundant in biological systems, their role in the supramolecular structure and phase transitions of Lipid-A has not been thoroughly investigated via experimental techniques. Only a handful of studies have been carried out for LPS membranes.<sup>38,41,47,50</sup> However, a comprehensive study using light scattering, quasielastic light scattering, small-angle X-ray scattering, transmission electron microscopy, scanning electron microscopy, conductivity measurements, and acid–base titrations revealed a higher degree of order for colloidal suspensions of Lipid-A in the presence of  $Ca^{2+}$  compared to  $Na^+$  ions in aqueous solutions.<sup>51</sup> In addition, structural factors for Lipid-A in the presence of  $Na^+$  ions were found to be similar to deionized Lipid-A suspensions.<sup>51</sup> The effect of  $Mg^{2+}$  concentration (a divalent cation), temperature, and pH on the supramolecular structure and phase behavior of Lipid-A has been previously investigated via small-angle X-ray diffraction, Fourier-transform infrared spectroscopy, and differential scanning calorimetry techniques.<sup>15–17,48</sup> These studies have shown that in the presence of  $Mg^{2+}$  cations and at temperatures below the phase transition  $T_c$ , Lipid-A aggregates occur simultaneously with lamellar and inverted cubic arrangements. An excess of  $Mg^{2+}$  ions from  $20^\circ$  to  $50^\circ$  C was overall observed to increase the stability of lamellar structures over samples of Lipid-A in pure water.<sup>15</sup> In agreement with the observations that divalent cations promote the stabilization of lamellar arrangements, our MD simulations show that  $Ca^{2+}$ -containing Lipid-A bilayers are stable at temperatures of 300 K and 328 K, whereas  $Na^+$ -containing Lipid-A membranes undergo a fast (after ca. 20 ns) transition to a nonlamellar suprastructure.

It is worth noting that the phase transition dependence with metal ions has not been observed in LPS membranes. LPS molecules contain several charged groups (phosphates of the Lipid-A moiety, the carboxylates of the KDO moieties, and phosphates attached to the heptose sugars) with one negative charge for each one of these functional groups and thus can

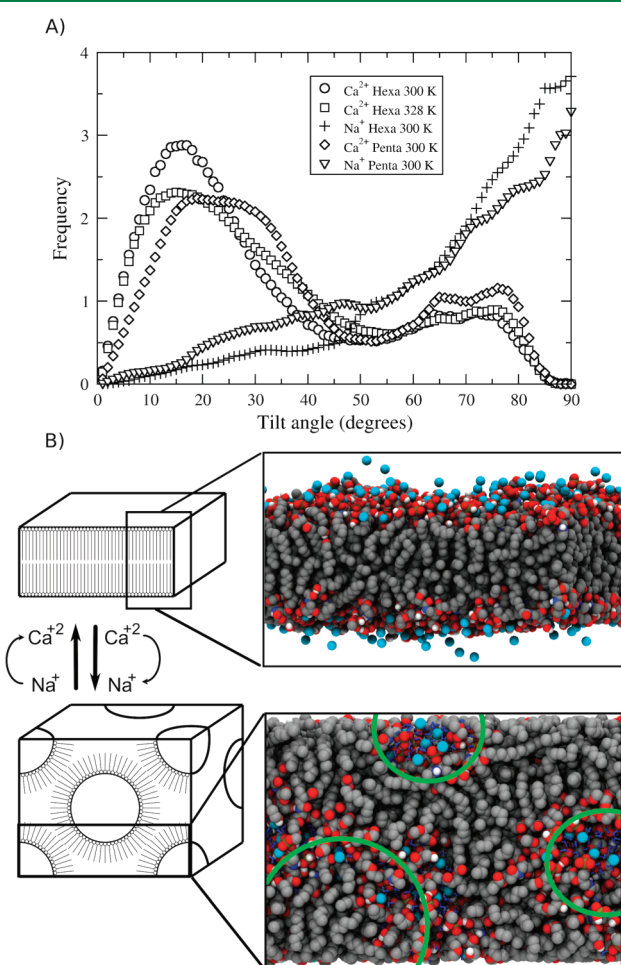


**Figure 8.** (A) Distribution of the molecular orientation of Lipid-A with respect to the  $z$  axis. Lipid-A alignment values to the  $z$  axis were averaged over the last 50 ns of simulation time for each system and range from  $0^\circ$  (parallel to the  $z$  axis) to  $90^\circ$  (perpendicular to the  $z$  axis). (B) Lamellar to nonlamellar transition scheme as a function of the replacement of  $Ca^{2+}$  by  $Na^+$  ions (left) and simulation snapshots ( $t = 1$  ns and  $t = 137$  ns) for the hexaacyl systems in the presence  $Na^+$  ions at 300 K (right). Molecular systems are represented in CPK model and atoms color-coded as follows: carbon, gray; oxygen, red; nitrogen, blue; hydrogen, white; and  $Na^+$  ions, cyan.

bind a larger number of “water shielding” cations compared to Lipid-A.<sup>41</sup> Therefore, it is plausible to expect hydration differences to be more accentuated for Lipid-A than for LPS. Recent neutron diffraction studies on the structure of multilamellar LPS membranes of *Pseudomonas aeruginosa* showed that water molecules penetrate the Na<sup>+</sup>-LPS membrane much deeper (up to  $\pm 14$  Å from the center of the bilayer) than the Ca<sup>2+</sup>-LPS membrane (up to  $\pm 22$  Å from the center of the bilayer).<sup>38</sup> The presence of Ca<sup>2+</sup> ions makes acyl chains in LPS membranes more ordered compared to Na<sup>+</sup> (and even Mg<sup>2+</sup>) cations.<sup>47</sup> In Lipid-A, counterions are chiefly located on the membrane surface as opposed to deeply embedded into the LPS membrane, thus being more accessible to Na<sup>+</sup>-water exchanges. As shown in the present simulations, each glucosamine phosphate coordinates only one Na<sup>+</sup>, which results in two cations being positioned relatively closely. The proximity of identical charges can favor the presence of screening water molecules, leading to gradual water penetration into the membrane, and ultimately to the lamellar  $\rightarrow$  nonlamellar transition (Figure 8B). The rigidifying effect of divalent cations is highest for Lipid-A with a less pronounced effect with increasing length of the sugar side chain within the LPS molecules.<sup>48</sup> The tight binding of Ca<sup>2+</sup> to glucosamine phosphate groups with  $k_d = 56-100 \mu\text{M}$  (though for its binding to KDO  $k_d = 6 \mu\text{M}$ )<sup>52</sup> makes water-cation exchange less favorable, resulting in a substantially more stable bilayer compared to Na<sup>+</sup>. Indeed, previous MD simulations of the smooth and rough LPS membranes in the presence of Ca<sup>2+</sup> have shown at the atomic level that this cation binds strongly to the phosphate and carboxylate groups in a cross-linked fashion and that water penetration was not significant within the time scale simulated.<sup>20,21,23</sup> Ca<sup>2+</sup> cations favor lamellar arrangements of smooth and rough LPS membranes at temperature ranges of 283.15–343.15 K and physiological water content.<sup>41,47</sup> Our results suggest a similar trend for Lipid-A membranes. Ca<sup>2+</sup> ions bind cross-linking two phosphate groups from distinct Lipid-A molecules functioning as “anchors” and consequently stabilizing the lamellar structure, as shown by the radial distribution function analyses.

Finally, to check for initial configurational bias, a second set of simulations was performed from scratch for each system using different initial Lipid-A orientations inside of the boxes. The new membranes were built using the same protocol described in the Methodology section. Each simulation was run for a total of 125 ns, and the last 50 ns was used for analyses. No significant differences were observed for the measured average properties presented as a function of the system setup, i.e., a maximum 3% difference between the two setups for any given average property value (data not shown for conciseness).

#### 4. CONCLUSIONS

Our glycolipid extension of the GROMOS force field was shown to satisfactorily reproduce a variety of available experimental measurements for Lipid-A membranes. Our results suggest that  $L\beta \rightarrow L\alpha$  transition in Lipid-A of *P. aeruginosa* takes place at lower temperatures than for most enterobacteria and that the type of (mono- versus divalent) cation has a greater effect on lamellar to nonlamellar transition than phenotypical variation within the liquid-crystalline phase. Furthermore, it has been previously shown that conformational ensemble and electrostatic properties of bacterial outer membrane proteins can differ significantly when simulated in lipid bilayers or their lipopolysaccharide counterparts.<sup>22,24</sup>

Therefore, the glycolipid membranes characterized here represent a more suitable platform for the study of outer membrane proteins in conjunction with the GROMOS force field.

#### ■ AUTHOR INFORMATION

##### Corresponding Author

\*E-mail: thereza.soares@ufpe.br or roberto.lins@ufpe.br.

##### Notes

The authors declare no competing financial interest.

#### ■ ACKNOWLEDGMENTS

This work was supported by the Brazilian National Council for Research and Development (CNPq), The State of Pernambuco Research Foundation (FACEPE), INCT-INAMI, nBioNet, Nanobiotec-BR/CAPES, and the Swedish Foundation for International Cooperation in Research and Higher Education (STINT). Computational resources were provided by the Environmental Molecular Sciences Laboratory at the Pacific Northwest National Laboratory.

#### ■ DEDICATION

This work is dedicated to Prof. Wilfred van Gunsteren on his 65th anniversary. T.A.S. and R.D.L. keep alive the same scientific enthusiasm conveyed by Prof. Wilfred van Gunsteren during their years of interaction.

#### ■ REFERENCES

- (1) Aderem, A.; Ulevitch, R. J. *Nature* **2000**, *406*, 782.
- (2) Underhill, D. M.; Ozinsky, A. *Curr. Opin. Immunol.* **2002**, *14*, 103.
- (3) Miller, S. I.; Ernst, R. K.; Bader, M. W. *Nat. Rev. Microbiol.* **2005**, *3*, 36.
- (4) Beutler, B.; Jiang, Z.; Georgel, P.; Crozat, K.; Croker, B.; Rutschmann, S.; Du, X.; Hoebe, K. *Annu. Rev. Immunol.* **2006**, *24*, 353.
- (5) Beutler, B.; Rietschel, E. T. *Nat. Rev. Immunol.* **2003**, *3*, 169.
- (6) Schromm, A. B.; Brandenburg, K.; Loppnow, H.; Moran, A. P.; Koch, M. H.; Rietschel, E. T.; Seydel, U. *Eur. J. Biochem.* **2000**, *267*, 2008.
- (7) Brandenburg, K.; Wiese, A. *Curr. Top. Med. Chem.* **2004**, *4*, 1127.
- (8) Raetz, C. R.; Reynolds, C. M.; Trent, M. S.; Bishop, R. E. *Annu. Rev. Biochem.* **2007**, *76*, 295.
- (9) Wilkinson, S. G. *Prog. Lipid Res.* **1996**, *35*, 283.
- (10) Brandenburg, K.; Kusumoto, S.; Seydel, U. *Biochim. Biophys. Acta* **1997**, *1329*, 183.
- (11) Brandenburg, K.; Hawkins, L.; Garidel, P.; Andra, J.; Muller, M.; Heine, H.; Koch, M. H.; Seydel, U. *Biochemistry* **2004**, *43*, 4039.
- (12) Gutsmann, T.; Schromm, A. B.; Brandenburg, K. *Int. J. Med. Microbiol.* **2007**, *297*, 341.
- (13) Chernomordik, L. V.; Zimmerberg, J.; Kozlov, M. M. *J. Cell Biol.* **2006**, *175*, 201.
- (14) Chernomordik, L. V.; Kozlov, M. M. *Annu. Rev. Biochem.* **2003**, *72*, 175.
- (15) Brandenburg, K. *Biophys. J.* **1993**, *64*, 1215.
- (16) Brandenburg, K.; Seydel, U. *Eur. J. Biochem.* **1990**, *191*, 229.
- (17) Brandenburg, K.; Seydel, U. *Eur. J. Biochem.* **1988**, *16*, 83.
- (18) Mueller, M.; Lindner, B.; Kusumoto, S.; Fukase, K.; Schromm, A. B.; Seydel, U. *J. Biol. Chem.* **2004**, *279*, 26307.
- (19) Lins, R. D.; Straatsma, T. P. *Biophys. J.* **2001**, *81*, 1037.
- (20) Lins, R. D.; Vorpagel, E. R.; Guglielmi, M.; Straatsma, T. P. *Biomacromolecules* **2008**, *9*, 29.
- (21) Soares, T. A.; Lins, R. D.; Straatsma, T. P. *J. Braz. Chem. Soc.* **2008**, *19*, 312.
- (22) Soares, T. A.; Straatsma, T. P. *AIP Conf. Proc.* **2007**, *963*, 1375.
- (23) Soares, T. A.; Straatsma, T. P. *Mol. Simul.* **2008**, in press.

- (24) Straatsma, T. P.; Soares, T. A. *Proteins: Struct., Funct., Genet.* **2009**, *74*, 475.
- (25) Lins, R. D.; Hunenberger, P. H. *J. Comput. Chem.* **2005**, *26*, 1400.
- (26) Berendsen, H. J. C.; Postma, J. P. M.; DiNola, A.; Haak, J. R. *J. Chem. Phys.* **1984**, 81.
- (27) Hockney, R. W. The potential calculation and some applications. In *Methods in Computational Physics*; Alder, B., Fernbach, S., Rotenberg, M., Eds.; Academic Press: New York/London, 1970; Vol. 9.
- (28) Bussi, G.; Donadio, D.; Parrinello, M. *J. Chem. Phys.* **2007**, *126*, 014101.
- (29) Hess, B.; Kutzner, C.; van der Spoel, D.; Lindahl, E. *J. Chem. Theory Comput.* **2008**, 4.
- (30) Franca, E. F.; Freitas, L. C.; Lins, R. D. *Biopolymers* **2011**, *95*, 448.
- (31) Franca, E. F.; Lins, R. D.; Freitas, L. C. G.; Straatsma, T. P. *J. Chem. Theory Comput.* **2008**, *4*, 2141.
- (32) Chandrasekhar, I.; Kastenholz, M.; Lins, R. D.; Oostenbrink, C.; Schuler, L. D.; Tielemans, D. P.; van Gunsteren, W. F. *Eur. Biophys. J.* **2003**, *32*, 67.
- (33) Oostenbrink, C.; Soares, T. A.; van der Vegt, N. F.; van Gunsteren, W. F. *Eur. Biophys. J.* **2005**, *34*, 273.
- (34) Berendsen, H. J. C.; Grigera, J. R.; Straatsma, T. P. *J. Phys. Chem.* **1987**, 91.
- (35) van Gunsteren, W. F.; Bakowies, D.; Baron, R.; Chandrasekhar, I.; Christen, M.; Daura, X.; Gee, P.; Geerke, D. P.; Glattli, A.; Hunenberger, P. H.; Kastenholz, M. A.; Ostenbrink, C.; Schenk, M.; Trzesniak, D.; van der Vegt, N. F. A. *Angew. Chem., Int. Ed.* **2006**, *45*, 4064.
- (36) van Gunsteren, W. F.; Bakowies, D.; Burgi, R.; Chandrasekhar, I.; Christen, M.; Daura, X.; Gee, P.; Glattli, A.; Hansson, T.; Oostenbrink, C.; Peter, C.; Pitera, J.; Schuler, L.; Soares, T. A.; Yu, H. B. *Chimia* **2001**, *55*, 856.
- (37) Abraham, T.; Schooling, S. R.; Nieh, M. P.; Kucerka, N.; Beveridge, T. J.; Katsaras, J. *J. Phys. Chem. B* **2007**, *111*, 2477.
- (38) Kucerka, N.; Papp-Szabo, E.; Nieh, M. P.; Harroun, T. A.; Schooling, S. R.; Pencer, J.; Nicholson, E. A.; Beveridge, T. J.; Katsaras, J. *J. Phys. Chem. B* **2008**, *112*, 8057.
- (39) Schindler, M.; Osbron, M. J. *Biochemistry* **1979**, *18*, 4425.
- (40) Brandenburg, K.; Funari, S. S.; Koch, M. H.; Seydel, U. *J. Struct. Biol.* **1999**, *128*, 175.
- (41) Snyder, S.; Kim, D.; McIntosh, T. J. *Biochemistry* **1999**, *38*, 10758.
- (42) Bedoux, G.; Vallee-Rehel, K.; Kooistra, O.; Zahringer, U.; Haras, D. *J. Mass Spectrom.* **2004**, *39*, 505.
- (43) Brandenburg, K.; Andra, J.; Muller, M.; Koch, M. H.; Garidel, P. *Carbohydr. Res.* **2003**, *338*, 2477.
- (44) Brandenburg, K.; Mayer, H.; Koch, M. H.; Weckesser, J.; Rietschel, E. T.; Seydel, U. *Eur. J. Biochem.* **1993**, *218*, 555.
- (45) Seydel, U.; Oikawa, M.; Fukase, K.; Kusumoto, S.; Brandenburg, K. *Eur. J. Biochem.* **2000**, *267*, 3032.
- (46) Brandenburg, K.; Matsuura, M.; Heine, H.; Muller, M.; Kiso, M.; Ishida, H.; Koch, M. H.; Seydel, U. *Biophys. J.* **2002**, *83*, 322.
- (47) Garidel, P.; Rappolt, M.; Schromm, A. B.; Howe, J.; Lohner, K.; Andra, J.; Koch, M. H. J.; Brandenburg, K. *Biochim. Biophys. Acta* **1999**, *1715*, 122.
- (48) Seydel, U.; Brandenburg, K.; Koch, M. H.; Rietschel, E. T. *Eur. J. Biochem.* **1989**, *186*, 325.
- (49) Brandenburg, K.; Koch, M. H.; Seydel, U. *J. Struct. Biol.* **1990**, *105*, 11.
- (50) Coughlin, R. T.; Haug, A.; McGroarty, E. J. *Biochemistry* **1983**, *22*, 2007.
- (51) Faunce, C. A.; Reichelt, H.; Paradies, H. H.; Quitschau, P.; Zimmermann, K. *J. Chem. Phys.* **2005**, *122*, 214727.
- (52) Schindler, M.; Osborn, M. J. *Biochemistry* **1979**, *18*, 4425.